arXiv:cond-mat/0205595v2 [cond-mat.supr-con] 21 Aug 2002

Shifts of the nuclear resonance in the vortex lattice in $YBa_2Cu_3O_7$

Pavel Lipavský and Jan Koláček
Institute of Physics, Academy of Sciences, Cukrovarnická 10, 16258 Praha 6, Czech Republic

Klaus Morawetz
Max Planck Institute for the Physics of Complex Systems, Noethnitzer Str. 38, 01187 Dresden, Germany

Ernst Helmut Brandt
Max-Planck-Institut für Metallforschung, D-70506 Stuttgart, Germany

The NMR and NQR spectra of ^{63}Cu in the CuO_2 plane of $YBa_2Cu_3O_7$ in the superconducting state are discussed in terms of the phenomenological theory of Ginzburg-Landau type extended to lower temperatures. We show that the observed spectra, Kumagai *et al.*, PRB **63**, 144502 (2001), can be explained by a standard theory of the Bernoulli potential with the charge transfer between CuO_2 planes and CuO chains assumed.

I. INTRODUCTION

Already in 1969 Rickayzen has derived the thermodynamic correction to the electrostatic Bernoulli potential in superconductors and has proposed to use this correction to study the pairing interaction.[1] Capacitive measurements of the Bernoulli potential have not shown any signal of this correction, however.[2–6] It turned out that the thermodynamic correction is cancelled by the surface dipole,[7] therefore, it can be accessed only by measurements probing the bulk of the superconductor. For a long time, there was no experimental method to fulfill this task so that the thermodynamic correction to the electrostatic potential and the related charge transfer have remained a theoretical topic[8–12] with no experimental justification.

The experiment aimed at the charge transfer in the bulk of the superconductor has been performed only recently. Kumagai, Nozaki and Matsuda[13] (KNM) reported very precise measurements of the nuclear magnetic resonance (NMR) and the nuclear quadrupole resonance (NQR) spectra for two high-T_c materials, a slightly overdoped $YBa_2Cu_3O_7$ and an underdoped $YBa_2Cu_4O_8$. Comparing NMR and NQR frequencies they found that the magnetic field, present in NMR while absent in NQR, causes changes of the electric field gradient (EFG) in the vicinity of the nucleus. In this way they first observed the charge transfer in the Abrikosov vortex lattice. They also pointed out that the conventional theory of the vortex charge completely fails to explain the experimental data giving a wrong sign and too small amplitude of the magnetic field effect on the EFG.

In this paper we discuss the KNM experiment in terms of a phenomenological theory of Ginzburg-Landau (GL) type proposed in Refs. 11,12. This theory is extended by features necessary to describe a layered structure of YBCO, in particular the CuO chains which serve as charge reservoirs. Unlike in a conventional superconductor, where the charge is transfered on a long distance from the vortex core to the region between the cores, in the YBCO the dominant role plays a local charge transfer between the CuO_2 planes and the CuO chains. This local transfer will be shown to explain the observed sign and amplitude of the magnetic field effect on the EFG. At low temperatures, there are two important corrections, the space variation of the magnetic field and the small but finite disorientation of the axis c in individual grains of the measured sample.

A. Electric field gradient effect in the vortex lattice

Let us briefly recall the experiment of Kumagai, Nozaki and Matsuda.[13] The ^{63}Cu atom in the CuO_2 plane subjected to the magnetic field, $B \parallel c$, with a number of holes, N, has NMR frequencies $\nu_1 = \gamma_{\rm Cu} B$ and

$$\nu_{2,3} = \gamma_{\rm Cu} B \mp (C + AN)\,. \tag{1}$$

The first term describes the coupling of the nuclear magnetic momentum to the magnetic field, $B = 9.4$ T in Ref. 13. The nucleus ^{63}Cu has spin 3/2 and its Zeeman coefficient is $\gamma_{\rm Cu} = 11.312$ MHz/T.

The second term of (1) is the EFG effect. The nucleus ^{63}Cu has a cigar shape elongated in the direction of its magnetic momentum and this electric quadrupole feels gradients of the electrostatic field due to a non-spheric charge of electrons and ions in its vicinity. The largest gradient of the electric field (the principal axis of the EFG tensor) is parallel to the axis c. The density dependent contribution to the EFG is attributed to the local interaction between nucleus with d-states on the Cu site. The experimental fit[14,13] to the EFG effect yields $C = 25$ MHz and $A = 34$ MHz per hole.

The NQR frequency includes the asymmetry correction, $\nu_{\rm NQR} = \nu_0\sqrt{1+\eta^2/3}$, where η is the difference between gradients in the a and b directions scaled to the gradient in the c direction. For the Cu atom in the plane of $YBa_2Cu_3O_7$ the a-b asymmetry is rather weak, $\sqrt{1+\eta^2/3} \approx 1 + 2.6 \times 10^{-4}$. The frequency ν_0 corresponds to the NMR in the zero magnetic field,

$\nu_0 = C + AN_0$, where N_0 is the number of holes in the superconducting non-magnetic state.

A combination of the resonance frequencies,

$$\Delta\nu = \nu_0 - \frac{1}{2}\left(\bar{\nu}_3 - \bar{\nu}_2\right), \tag{2}$$

would be zero if the magnetic field has no effect on the number of holes on the Cu sites. Actually, this is the case for temperatures above T_c. Below the critical temperature, the shift $\Delta\nu$ is non-zero indicating changes of the quadrupole coupling due to the effect of the magnetic field on the hole density. Briefly, $\Delta\nu$ serves as a sensor of the charge transfer in the Abrikosov vortex lattice.[13]

B. Charge transfer between chains and planes

In this paper we evaluate the shift $\Delta\nu$. To motivate our approach we want to recall the way in which the experimental data are obtained. The measurement yields distributions $F_{2,3}(\nu)$ of the NMR frequencies, see Fig. 3 in Ref. 13. The frequencies $\bar{\nu}_{3,2}$, used by KNM in formula (2) are positions of the maxima of $F_{2,3}(\nu)$. Since NMR lines have a finite width Γ, each site of a local frequency $\nu_{2,3}(\mathbf{r})$ contributes to the spectrum by the Lorentzian

$$F_i(\nu) = \left\langle \frac{\Gamma}{(\nu-\nu_i)^2+\Gamma^2} \right\rangle \equiv \frac{1}{\Omega}\int d\mathbf{r} \frac{\Gamma}{(\nu-\nu_i(\mathbf{r}))^2+\Gamma^2}. \tag{3}$$

The integral runs over the 2D volume, $\Omega = \int d\mathbf{r}$, covering the elementary cell of the Abrikosov vortex lattice. The magnetic field B and the density N are functions of $\mathbf{r}$, the frequencies $\nu_{2,3}$ depend on $\mathbf{r}$ via (1). The experimental magnetic field is the mean value, $B = \langle B \rangle$.

The finite line width is crucial for the interpretation of the KNM experiment. The observed contributions of the quadrupole shifts are less than 25 kHz which is much smaller than the width of the spectral line $\Gamma \approx 140$ kHz. In this limit, the maximum of the spectral line is given by the mean value and the lowest statistical variations,

$$\bar{\nu}_i = \langle \nu_i \rangle - \frac{2\left\langle (\nu_i - \langle \nu_i \rangle)^3 \right\rangle}{\Gamma^2 - 6\left\langle (\nu_i - \langle \nu_i \rangle)^2 \right\rangle}. \tag{4}$$

The variations are important at low temperatures due to a strong compression of the magnetic field in vortex cores resulting in a strong space-dependence of the Zeeman effect. Close to the critical temperature the variations vanish and the maxima of the NMR lines approach the mean frequencies, $\bar{\nu}_{2,3} \approx \langle \nu_{2,3} \rangle$. Close to T_c one finds from (1) and (2) that

$$\Delta\nu \approx A\left(N_0 - \langle N \rangle\right). \tag{5}$$

According to (5), the shift $\Delta\nu$ reflects how many holes have been removed from the CuO_2 plane. The in-plane charge transfer contributes only via variations giving, as shown below, a negligible correction at all temperatures.

C. Plan of the paper

The physical picture we assume here is based on properties of the non-magnetic state of YBCO. The superconducting state appears mainly in CuO_2 planes, in chains the gap is induced by the proximity effect. The transition to the superconducting state shifts the chemical potential in the same manner as in conventional superconductors.[10,12] This shift is large in planes, where the pairing mechanism is located, while it is negligible in chains. In equilibrium the electrochemical potential is constant so the unequal shift of the chemical potential results in the charge transfer between plains and chains, until the equilibrium condition is established by the electrostatic potential.

The magnetic field partially suppresses the superconducting component what leads to a partial backward charge transfer. In the numerical treatment we assume both mechanisms, the transfer between chains and planes and the in-plane transfer. We show that this backward transfer between chains and planes brings the dominant contribution to the shift $\Delta\nu$.

In the next section we introduce the Lawrence-Doniach model of the layered superconductor. In Sec. III we derive a set of equations for the GL function, the vector potential, and the electrostatic potential. The charge density is obtained from the Poisson equation adapted to the layered structure. In the Sec. IV we evaluate the distributions $F_{2,3}(\nu)$ from the frequencies $\nu_{2,3}(\mathbf{r})$ given by (1) with the theoretical values of $B(\mathbf{r})$ and $N(\mathbf{r})$ obtained from the extended GL theory[12]. In Sec. V we present numerical results and discuss the individual contributions to the experimental data. We show that the approximation (5) applies close to the critical temperature, but at low temperatures the space variation of the magnetic field leads to appreciable corrections. In Subsec. C we compare our results with the model for conventional (not layered) superconductors and explain why the conventional model results in the reversed sign and too small amplitude of the line shift. In Subsec. D we include a correction for samples made of c-oriented grains and show that the deviations from the ideal orientation are important at low temperatures. Sec. VI contains a summary.

II. LAWRENCE-DONIACH MODEL

The model of layered superconductors has been proposed by Lawrence and Doniach[15], see also Ref. 16. We associate the direction z with the c axis of the YBCO and introduce a layer index j and an additional index $\pm$ which specifies the CuO_2 layer position, $z_j^{\pm} = jD \pm \frac{1}{2}D_{pp}$, where $D = 11.65$ Å is the period along the axis c and $D_{pp} = 3.17$ Å is the distance between two neighboring planes. Positions of layers of chains are $z_j^c = jD + \frac{1}{2}D$.

In the spirit of the tight-binding description, the variable z is replaced by the layer index. The wave function becomes a function of the layer index, $\psi(x,y,z) \to \psi_j^{\pm,c}(\mathbf{r})$, and the 2D coordinate $\mathbf{r} \equiv (x,y)$.

A. Kinetic energy

The kinetic energy is composed of parts parallel to the planes and the Josephson coupling along the c axis. The kinetic part of the free energy for the motion in the layer is treated within the isotropic effective mass,

$$f_{\rm kin}^{j\iota} = \frac{1}{2m_\iota^*} \left| \left(-i\hbar\nabla - e^* \mathbf{A}_j^\iota \right) \psi_j^\iota \right|^2 , \qquad (6)$$

where $\mathbf{A}_j^\iota$ is the in-plane component of the 3D vector potential $\mathbf{A}(x,y,z_j^\iota)$. The masses in both planes are identical, $m_\pm^* = m_p^*$. For simplicity we assume the 2D effective mass m_c^* in the chain layer to be isotropic, too.

The motion between layers is represented by the Josephson coupling,

$$\begin{aligned} f_{\rm kin}^{j,+-} &= J_{pp} \left| \psi_j^+ - {\rm e}^{-i\theta_j^{+-}} \psi_j^- \right|^2 , \\ f_{\rm kin}^{j,c+} &= J_{cp} \left| \psi_j^c - {\rm e}^{-i\theta_j^{c+}} \psi_j^+ \right|^2 , \\ f_{\rm kin}^{j,-c} &= J_{cp} \left| \psi_j^- - {\rm e}^{-i\theta_j^{-c}} \psi_{j-1}^c \right|^2 . \end{aligned} \qquad (7)$$

The phase factors θ of the off-diagonal terms are given by the c-component of the 3D vector potential. For $\mathbf{B} \parallel c$ we can use a gauge in which the c component of the vector potential is zero. In this gauge, all three phases are zero, $\theta_j^{\iota\iota'} = 0$. The total kinetic free energy is a sum over all layers, $\mathcal{F}_{\rm kin} = \int d\mathbf{r} \sum_{j,\iota} (f_{\rm kin}^{j\iota} + f_{\rm kin}^{j,\iota\iota'})$.

B. Condensation energy

Following Bardeen[17,18] we use the Gorter-Casimir free energy to describe the condensation. We assume that the energy released by the formation of Cooper pairs is located in CuO$_2$ planes. In terms of the wave function the contribution of planes to the free energy reads[12]

$$f_{\rm con}^{j\pm} = -\varepsilon_{\rm con} \varpi_j^\pm - \frac{1}{2}\gamma_p T^2 \sqrt{1-\varpi_j^\pm}, \qquad (8)$$

where γ_p is the plane contribution to Sommerfeld's γ (linear coefficient of the electronic specific heat), and

$$\varpi_j^\pm = \frac{2|\psi_j^\pm|^2}{2|\psi_j^\pm|^2 + n_{\rm nor}^{j,\pm}} \qquad (9)$$

is the fraction of superconducting holes in the given plane. The denominator of (9) is the total density of pairable holes, $n_j^\iota = 2|\psi_j^\iota|^2 + n_{\rm nor}^{j,\iota}$, which is a sum of the superconducting density and the density of normal holes.

In the chains we treat the condensation energy as negligible. The free energy thus includes only the contribution due to the reduced entropy, $f_{\rm con}^{jc} = -\frac{1}{2}\gamma_c T^2 \sqrt{1-\varpi_j^c}$. The meaning of symbols is analogous to the case of planes. Again, the sum over all layers reads $\mathcal{F}_{\rm con} = \int d\mathbf{r} \sum_{j\iota} f_{\rm con}^{j\iota}$.

C. Coulomb interaction

The total density of holes is linked to the 2D density of charge, $\rho_j^\iota = e n_j^\iota + \rho_{\rm latt}^\iota$, which creates the electrostatic potential,

$$\varphi_j^\iota(\mathbf{r}) = \frac{1}{4\pi\epsilon} \int d\mathbf{r}' \sum_{j'\iota'} \frac{\rho_{j'}^{\iota'}(\mathbf{r}')}{\sqrt{|\mathbf{r}'-\mathbf{r}|^2 + (z_{j'}^{\iota'} - z_j^\iota)^2}} . \qquad (10)$$

The Coulomb energy is $\mathcal{F}_C = \frac{1}{2}\int d\mathbf{r} \sum_{j\iota} \rho_j^\iota \varphi_j^\iota$.

It is advantageous to treat the electrostatic potential in the momentum representation,

$$\varphi_\iota(\mathbf{k}) = \int d\mathbf{r}\, \varphi_\iota(\mathbf{r})\, {\rm e}^{-i\mathbf{k}\mathbf{r}} . \qquad (11)$$

We have moved the superscript ι into subscript and lifted the index j since all equivalent layers are at identical potentials, $\varphi_j^\iota = \varphi_m^\iota$. The electrostatic potential then reads

$$\varphi_\iota(\mathbf{k}) = \frac{1}{\epsilon D} \sum_{\iota'} L_{\iota\iota'}^{-1} \rho_{\iota'}(\mathbf{k}), \qquad (12)$$

with elements of the inverse Laplace operator

$$\begin{aligned} L_{++}^{-1} = L_{--}^{-1} = L_{cc}^{-1} &= \frac{D}{2k} \frac{1+{\rm e}^{-kD}}{1-{\rm e}^{-kD}} \\ L_{+-}^{-1} = L_{-+}^{-1} &= \frac{D}{2k} \frac{{\rm e}^{-kD_{pp}} + {\rm e}^{-k(D-D_{pp})}}{1-{\rm e}^{-kD}} \\ L_{c\pm}^{-1} = L_{\pm c}^{-1} &= \frac{D}{2k} \frac{{\rm e}^{-kD_{cp}} + {\rm e}^{-k(D_{cp}+D_{pp})}}{1-{\rm e}^{-kD}} . \end{aligned} \qquad (13)$$

Here $D_{cp} = \frac{1}{2}(D - D_{pp})$ denotes the distance between adjacent chains and planes.

When inverted, the relation (12) yields the density of charge in terms of the electrostatic potential,

$$\rho_\iota(\mathbf{k}) = \epsilon D \sum_{\iota'} L_{\iota\iota'} \varphi_{\iota'}(\mathbf{k}). \qquad (14)$$

In our approach the electrostatic potential is evaluated from the request of constant electrochemical potential, and the relation (14) is used to evaluate the charge transfer.

III. EQUATIONS OF MOTION

The total free energy is the sum of the components discussed above and the Helmholtz free energy of the magnetic field, $\mathcal{F}_M = \int d\mathbf{r}dz \frac{1}{2\mu_0}(\mathbf{B} - \mathbf{B}_0)^2$. Note that the magnetic energy does not have a layered structure but it is given by a 3D integration. The magnetic field is the 3D rotation of the vector potential, $\mathbf{B} = \mathrm{rot}\mathbf{A}$.

The total free energy, $\mathcal{F} = \mathcal{F}_{\mathrm{kin}} + \mathcal{F}_{\mathrm{con}} + \mathcal{F}_C + \mathcal{F}_M$, is a functional of the wave function ψ, the vector potential $\mathbf{A}$ and the normal density n_{nor}. By variations with respect to these functions one arrives at equations of motion. For the conventional superconductor, this procedure is described in Ref. 12. We do not present its straightforward modification for the layered structure but discuss directly the results.

A. Maxwell equation

The functional variation $\delta\mathcal{F}/\delta\mathbf{A}$ yields the Maxwell equation,

$$\nabla^2\mathbf{A} = -\mu_0 \sum_{j\iota} \delta(z - z_j^\iota)\,\mathbf{j}_j^\iota. \tag{15}$$

The right hand side includes the in-plane 2D currents,

$$\mathbf{j}_j^\iota = \frac{e^*}{m_\iota^*}\mathrm{Re}\,\bar{\psi}_j^\iota \left(-i\hbar\nabla - e^*\mathbf{A}_j^\iota\right)\psi_j^\iota. \tag{16}$$

In principle, Josephson currents in the c direction may be also present. From the translational and mirror symmetries it follows that no Josephson currents flow between two neighboring CuO$_2$ planes. Assuming very small Josephson coupling between the chains and planes we neglect also the current between these layers.

The Maxwell equation (15) has the integral form

$$\mathbf{A}(\mathbf{r}, z) = \frac{\mu_0}{4\pi}\int d\mathbf{r}' \sum_{j'\iota'} \frac{\mathbf{j}_{j'}^{\iota'}(\mathbf{r}')}{\sqrt{|\mathbf{r}' - \mathbf{r}|^2 + (z_{j'}^{\iota'} - z)^2}}. \tag{17}$$

For $z = z_j^\iota$ the vector potential in the Fourier representation simplifies to

$$\mathbf{A}_\iota(\mathbf{k}) = \frac{\mu_0}{D}\sum_{\iota'} L_{\iota\iota'}^{-1}\mathbf{j}_{\iota'}(\mathbf{k}). \tag{18}$$

For the YBCO with its large London penetration depth, $\lambda_{\mathrm{Lon}} = 14000$ Å, the vector potential changes only negligibly along the c axis. Indeed, the applied magnetic field 9.4 T results in a vortex distance of 157 Å, which is small compared to λ_{Lon}. The space modulation of the magnetic field is thus covered by the lowest Fourier components of the Abrikosov lattice. Since the vortex distance is large on the scale of the YBCO lattice constant D, one can take the long wave length limit, $k \to 0$, in which (18) reads

$$\mathbf{A}(\mathbf{k}) = \frac{\mu_0}{k^2}\mathbf{j}(\mathbf{k}), \qquad \mathbf{j}(\mathbf{k}) = \frac{1}{D}\sum_{\iota'}\mathbf{j}_{\iota'}(\mathbf{k}). \tag{19}$$

In the approximation (19) the vector potential is identical in chain and plane layers so that we can skip its index.

B. Schrödinger equation

The Schrödinger equation of a system consisting of three periodically repeated layers has a complicated notation. We first write down this equation in its general form and then reduce it by symmetries and the approximation of weak Josephson coupling between chains and planes. The result oriented reader can skip reading details of the equations in this section.

The variation $\delta\mathcal{F}/\delta\bar{\psi}_j^\iota$ results in the set of Lawrence-Doniach equations

$$\begin{aligned}
&J_{pp}\left(\psi_j^+ - \psi_j^-\right) + J_{cp}\left(\psi_j^+ - \psi_j^c\right)\\
&+ \frac{1}{2m_p^*}\left(-i\hbar\nabla - e^*\mathbf{A}\right)^2\psi_j^+ + \chi_j^+\psi_j^+ = 0,\\
&J_{pp}\left(\psi_j^- - \psi_j^+\right) + J_{cp}\left(\psi_j^- - \psi_{j-1}^c\right)\\
&+ \frac{1}{2m_p^*}\left(-i\hbar\nabla - e^*\mathbf{A}\right)^2\psi_j^- + \chi_j^-\psi_j^- = 0,\\
&J_{cp}\left(\psi_j^c - \psi_{j+1}^-\right) + J_{cp}\left(\psi_j^c - \psi_j^+\right)\\
&+ \frac{1}{2m_c^*}\left(-i\hbar\nabla - e^*\mathbf{A}\right)^2\psi_j^c + \chi_j^c\psi_j^c = 0.
\end{aligned} \tag{20}$$

We have used zero phases of the Josephson terms.

For $\mathbf{B} \parallel c$, all CuO$_2$ planes are identical, therefore, $\psi_j^+ = \psi_j^- = \psi_{j+1}^- \equiv \psi_p$. The chain layers are also identical, $\psi_j^c = \psi_{j-1}^c \equiv \psi_c$. This simplifies the set (20) to two 2D Schrödinger equations

$$\begin{aligned}
J_{cp}\left(\psi_p - \psi_c\right) + \frac{1}{2m_p^*}\left(-i\hbar\nabla - e^*\mathbf{A}\right)^2\psi_p + \chi_p\psi_p = 0,\\
2J_{cp}\left(\psi_c - \psi_p\right) + \frac{1}{2m_c^*}\left(-i\hbar\nabla - e^*\mathbf{A}\right)^2\psi_c + \chi_c\psi_c = 0.
\end{aligned} \tag{21}$$

The effective potentials,

$$\begin{aligned}
\chi_p &= -2\frac{\varepsilon_{\mathrm{con}}}{n_p} + \frac{\gamma_p T^2}{2n_p}\frac{1}{\sqrt{1 - \frac{2|\psi_p|^2}{n_p}}},\\
\chi_c &= \frac{\gamma_c T^2}{2n_c}\frac{1}{\sqrt{1 - \frac{2|\psi_c|^2}{n_c}}},
\end{aligned} \tag{22}$$

follow from the variation of the condensation energy. The potential in chains consists of the entropy term only.

If one neglects the effect of the charge transfer on the material parameters $(n_p, n_c, \varepsilon_{\mathrm{con}}, \gamma_p, \gamma_c)$, the set of equations (19) and (21-22) is closed. As in the ordinary GL theory this set describes the magnetic properties of the system. In fact, the transfered density of holes is very small compared to the total densities n_p and n_c. Therefore in the first step, the magnetic field $\mathbf{B}$ and the wave function ψ can be evaluated from this set with no regards to the electrostatic phenomena. The charge transfer is evaluated in the second step from the wave function ψ.

C. Electrostatic potential

From variations of the free energy with respect to the normal densities $n_{\rm nor}^{p,c}$ one finds the electrostatic potential[12]

$$e\varphi_p = \chi_p \frac{|\psi_p|^2}{n_p} + \frac{T^2}{2}\frac{\partial \gamma_p}{\partial n_p}\sqrt{1-\frac{2|\psi_p|^2}{n_p}} + \frac{\partial \varepsilon_{\rm con}}{\partial n_p}\frac{2|\psi_p|^2}{n_p}$$

$$e\varphi_c = \chi_c \frac{|\psi_c|^2}{n_c} + \frac{T^2}{2}\frac{\partial \gamma_c}{\partial n_c}\sqrt{1-\frac{2|\psi_c|^2}{n_c}}\ . \qquad (23)$$

The right hand sides represent local changes of the chemical potential. Equations (23) thus express that the electrochemical potential remains constant.

One can see that the electrostatic potential in planes differs from the potential in chains. At first glance, these potentials differ by the term

$$\frac{\partial \varepsilon_{\rm con}}{\partial n_p} \approx \frac{T_c^2}{4}\frac{\partial \gamma_p}{\partial n_p} + \frac{\gamma_p T_c}{2}\frac{\partial T_c}{\partial n_p}. \qquad (24)$$

We have used the Gorter-Casimir formula for the condensation energy, $\varepsilon_{\rm con} = \frac{1}{4}\gamma_p T_c^4$ and the assumption that the thermodynamic properties of the superconducting phase are dominated by planes.

For YBCO the term (24) is much larger than any other term in the set (23). This is due to a rather strong dependence of the critical temperature T_c on the density of holes in planes. Blatter's approximation[10] of the electrostatic potential includes the second term of (24) only. For simplicity we use Blatter's approximation by taking

$$\varphi_p = \frac{\gamma_p T_c}{e}\frac{\partial T_c}{\partial n_p}\frac{|\psi_p|^2}{n_p}, \qquad \varphi_c = 0. \qquad (25)$$

Using approximation (25) in the Poisson equation (14) one obtains the 2D density of holes needed to evaluate the electric field gradient effect on the NMR lines.

D. Limit of weak Josephson coupling

Within the approximation (25) the electrostatic potential depends only on the wave function in planes. For a weak coupling between chains and planes, $J_{cp} \to 0$, the set of two non-linear equations (21) simplifies to a single equation,

$$\frac{1}{2m_p^*}\left(-i\hbar\nabla - e^*\mathbf{A}\right)^2\psi + \chi_p\psi = 0. \qquad (26)$$

We have introduced a 3D wave function $\psi = \sqrt{\frac{2}{D}}\psi_p$, in terms of which the current $\mathbf{j}$ has the usual GL form

$$\mathbf{j} = \frac{e^*}{m_p^*}{\rm Re}\,\bar\psi\left(-i\hbar\nabla - e^*\mathbf{A}\right)\psi. \qquad (27)$$

The wave function ψ corresponds to the 3D density of pairable holes, $n = 2n_p/D$. As one expects, in the limit of weak Josephson coupling, the magnetic properties are described by the customary GL theory.

To summarize our approach, we use the numerical code developed originally as a solver of the GL equations.[19] Its modification to the Bardeen's approximation has been discussed in Ref. 12. The output is the magnetic field $\mathbf{B}$ and the wave function ψ. The wave function is scaled to its layered counterpart ψ_p and used in (25) to provide us with the electrostatic potential in planes. From the Poisson equation (14) we obtain the density of holes in the CuO$_2$ planes as

$$\rho_p(\mathbf{k}) = \frac{2k\epsilon\left(1+{\rm e}^{-kD}\right)}{\left(1-{\rm e}^{-2kD_c}\right)\left(1+{\rm e}^{-kD_{\rm int}}\right)}\varphi_p(\mathbf{k}). \qquad (28)$$

In our numerical treatment below we use the full expression (28). It should be noted, however, that the long wave length limit $k \to 0$, i.e., $\rho_p(\mathbf{k}) = \frac{\epsilon}{D_c}\varphi_p(\mathbf{k})$, gives nearly the same result. As the relative errors due to the long wave length approximation are of the order of 10^{-3}, one can say that the charge is transferred locally from planes to chains. If the charge of planes and chains in the vortex core is summed together, the vortex cores remain nearly neutral.

IV. ELECTRIC FIELD GRADIENT EFFECT

Now we are ready to evaluate the NMR lines. The energy levels of the nucleus with spin $I = 3/2$ and spin component along the magnetic field, $m = -3/2, -1/2, 1/2, 3/2$, read[20]

$$E_m = -\hbar\gamma_{\rm Cu}Bm + \frac{e^2qQ}{12}\left(1-\frac{3}{2}\sin^2\theta\right)\left(3m^2-\frac{15}{4}\right). \qquad (29)$$

Here Q is the quadrupole moment of the nucleus, q is the EFG which depends on the transfered charge, and θ is the angle between the principal axis of the EFG tensor and the magnetic field.

The NMR frequencies are differences between neighboring levels, $\hbar\nu_1 = E_{-1/2} - E_{1/2}$, $\hbar\nu_2 = E_{1/2} - E_{3/2}$, and $\hbar\nu_3 = E_{-3/2} - E_{-1/2}$. The empirical formula (1) corresponds to the magnetic field parallel to the axis c. When the magnetic field declines from the axis c by angle θ, the EFG effect on the NMR frequencies is reduced,

$$\nu_{2,3} = \gamma_{\rm Cu}B \mp (C + AN)\left(1-\frac{3}{2}\sin^2\theta\right). \qquad (30)$$

The amplitude of the local magnetic field changes in space, $B = \langle B\rangle + \Delta B$. Although the deviations ΔB from the mean field are rather small, they bring an appreciable contribution to the NMR frequencies on the scale of the shift $\Delta\nu$. The EFG effect depends on the angle θ given by disorientations of grains in the sample. In the appendix we show that the contribution of the magnetic field perpendicular to the axis c which appears even in a perfectly oriented crystal due to the layered nature of diamagnetic currents is negligible.

For a quantitative discussion of the EFG effect, it is advantageous to compare the NMR frequency with its value in the absence of diamagnetic currents, $\nu_{2,3} = \nu_{2,3}^{\rm ref} + \Delta\nu_{2,3}$, where

$$\nu_{2,3}^{\rm ref} = \gamma_{\rm Cu}\langle B\rangle \mp AN_0. \tag{31}$$

The deviation caused by the diamagnetic currents and the disorientation is

$$\Delta\nu_{2,3} = \gamma_{\rm Cu}\Delta B \mp \left(A\Delta N - \nu_0\frac{3}{2}\sin^2\theta\right). \tag{32}$$

The density of holes per Cu site needed in (32) is proportional to the charge density in the planes (28),

$$\Delta N(\mathbf{r}) = \frac{\Omega_{\rm Cu}}{e}\left(\rho_p(\mathbf{r}) - \rho_p^0\right), \tag{33}$$

where $\Omega_{\rm Cu} = 14.88$ Å^2 is the area per Cu atom in a single plane. The density ρ_p^0 describes the transfer of holes in the non-magnetic state. Since the non-magnetic state is isotropic, i.e., it has only the component $k = 0$, from (25) and (28) one finds

$$\rho_p^0 = \frac{\epsilon}{D}\frac{|\psi_\infty|^2}{n_p^2}\gamma_p T_c^2\frac{\partial\ln T_c}{\partial\ln n_p}, \tag{34}$$

where $|\psi_\infty|^2 = \frac{1}{2}(1-t^4)n_p$ is the non-magnetic value of the GL function in Bardeen's model, $t = T/T_c$.

A. Average over grain orientation

So far we have discussed a single crystal. The sample measured by KNM[13] is made, however, from c oriented grains. Of course, there is a small but finite scatter in the orientation of individual grains. The angle θ then varies from grain to grain keeping its value independent of the temperature and the magnetic field, provided that the applied magnetic field is parallel to the mean orientation. The observed NMR lines are the average over all grains.

We assume that the azimuthal and the polar angles θ and ϕ are given by the Boltzmann distribution,

$$f(\theta,\phi) \propto \exp\left(-\frac{E_{\rm or}}{k_B T_{\rm prep}}\sin^2\theta\right), \tag{35}$$

where $E_{\rm or}$ is the energy needed to disorient the grain during a preparation at temperature $T_{\rm prep}$. One can integrate out the polar angle,

$$f(\theta) \propto \sin(\theta)\exp\left(-\frac{E_{\rm or}}{k_B T_{\rm prep}}\sin^2\theta\right). \tag{36}$$

For $E_{\rm or} \gg k_B T_{\rm prep}$, which is a necessary condition to prepare a well oriented sample, the large angles are very unlikely and one can use the approximation

$$f(\theta) = \frac{2}{\theta_c}\theta\,{\rm e}^{-\theta^2/\theta_c^2}, \tag{37}$$

where $\theta_c^2 = k_B T_{\rm prep}/E_{\rm or}$ measures the scatter of angles.

The average over the orientation of grains has to be performed in addition to the natural line width. The observed distribution of frequencies thus reads,

$$\bar F_{2,3}(\nu) = \int_0^{\frac{\pi}{2}} d\theta\, f(\theta)\int d\mathbf{r}\frac{\Gamma}{(\nu - \nu_{2,3}(\theta,\mathbf{r}))^2 + \Gamma^2}, \tag{38}$$

where $\nu_{2,3}$ is given by (31) and (32).

The integral over θ in (38) can be evaluated analytically in terms of the exponential integral of complex arguments. This step, however, is not favorable numerically. A faster numerical scheme is obtained if one first evaluate the distribution $F_{2,3}$ of an ideally oriented sample via (3) with the NMR frequency of a perfectly aligned magnetic field (1). The angular averaging is then covered by a convolution,

$$\bar F_{2,3}(\nu) = \int_0^{\frac{\pi^2}{4\theta_c^2}} dx\,{\rm e}^{-x} F_{2,3}\left(\nu \mp \frac{3}{2}\nu_0\theta_c^2 x\right). \tag{39}$$

From the experimental data of KNM we estimate $\Gamma \approx 140$ kHz and $\frac{3}{2}\nu_0\theta_c^2 = 0.9\Gamma = 126$ kHz. For these values the maximum of the lower NMR frequency is shifted by 78.3 kHz while the maximum of the upper frequency is shifted by -78.3 kHz. This shift appears at any temperature and it is subtracted in the evaluation of the EFG effect. The upper integration limit, $\pi^2/4\theta_c^2 \approx 10^3$, can be replaced by infinity or a smaller cut off at convenience.

V. NUMERICAL RESULTS

Our numerical treatment follows the three steps mentioned above. In the first step we evaluate the GL function $\psi(\mathbf{r})$ and the magnetic field $B(\mathbf{r})$ of the Abrikosov vortex lattice using Bardeen's extension of the GL theory represented by the set of equations (19,26-27). In this step we take the magnetic field as parallel to the axis c neglecting its small perpendicular component in individual grains.

In the second step we use Blatter's approximation (25) to evaluate the electrostatic potential in planes from the wave function. The charge density is obtained from the Poisson equation (28) and is rescaled to the transfered number $N(\mathbf{r})$ of holes per Cu site via (33).

In the third step we evaluate the local NMR frequencies for the magnetic field parallel to the axis c using (32) with $\theta = 0$. The distribution F of the NMR frequencies for a single crystal with $\mathbf{B} \parallel c$ is obtained via space averaging of Lorentzian lines (3). The distribution $\bar{F}$ of the NMR frequencies for the granular sample is obtained from F via the convolution (39). The maximum frequencies $\bar{\nu}_{2,3}$ of the crystal and granular samples are found from the maxima of $F_{2,3}$ and $\bar{F}_{2,3}$, respectively. The latter one can be compared with the experimental results of KNM, the former represents our prediction for similar measurements that, as we hope, will be performed on single crystals in future.

The material parameters of the $YBa_2Cu_3O_7$ from Ref. 21 are: the density of pairable holes $n = 5 \times 10^{27}$ m^{-3}, the effective mass $m_p^* = 6.92\, m_e$, the critical temperature $T_c = 90$ K, and the Sommerfeld constant $\gamma_p = 302$ JK^{-2}m^{-3}. These values give a London penetration depth $\lambda_{\rm Lon} = 1.4 \times 10^{-7}$ m, an upper critical field $B_{c2} = 96.5$ T, and a GL parameter at the critical temperature $\kappa_0 = 55$. In Fig. 2.16 Plakida[21] shows results of Junod[22] according to which the charge transfer $-0.03\, e$ from chains to planes per Cu site leads to a decrease of the critical temperature by 30 K. This corresponds to $\partial \ln T_c / \partial \ln n_p = -4.82$. We take the permittivity $\epsilon = 4\epsilon_0$. We do not discuss the $YBa_2Cu_4O_8$ for which we could not find relevant material parameters.

A. Space variation of the NMR frequency

Figure 1 shows the fishnet plot of the lower NMR frequency $\Delta\nu_2(\mathbf{r})$ for $T = 0.6\ T_c$ and $\theta = 0$. The variation is of the order of 100 kHz, which is comparable to the line width.

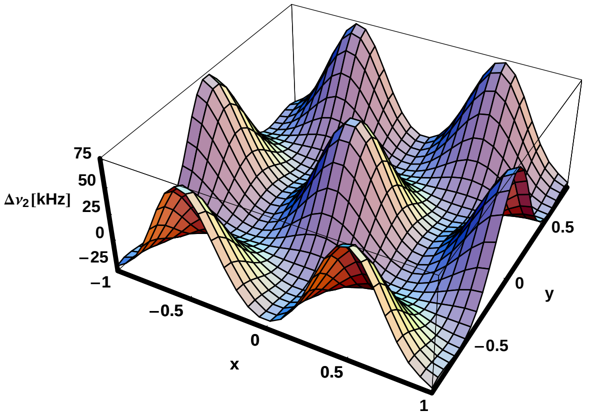

FIG. 1. The lower NMR frequency $\Delta\nu_2(\mathbf{r})$ in the crystal at $T = 0.6\ T_c$. The frequency reflects the triangular structure of the Abrikosov lattice. The maxima are at the vortex cores.

In Fig. 2 we plot the contribution of the Zeeman effect, $\Delta\nu_{\rm Z} = \gamma_{\rm Cu}\Delta B$, and the EFG effect, $\Delta\nu_{\rm EFG} = -A\Delta N$ separately. One can see that the Zeeman effect is about seven times larger that the EFG effect. The main contribution to the spatial variation of the NMR frequency is thus due to the compression of the magnetic field in vortex cores. On the other hand, the EFG has nonzero mean values, therefore, it contributes more to the observable shift of the maxima of the NMR line.

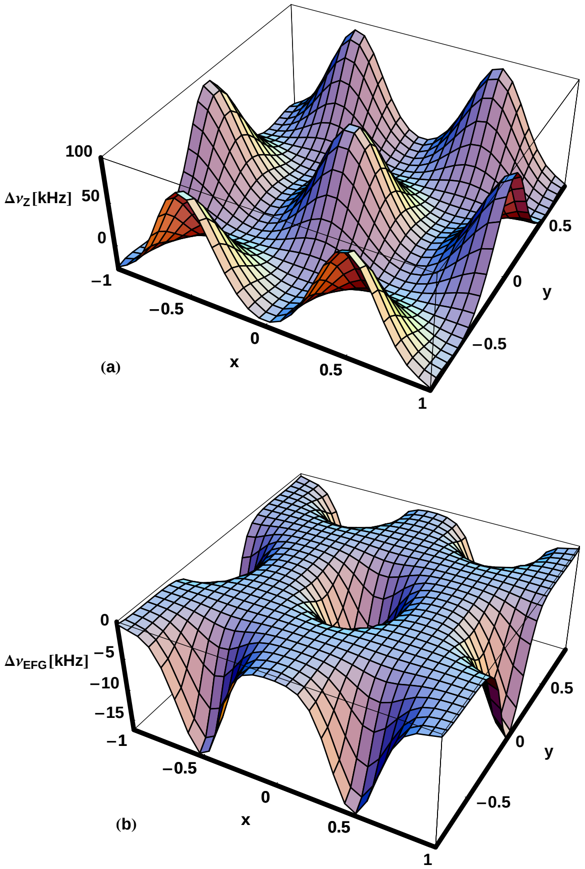

FIG. 2. The Zeeman effect $\Delta\nu_{\rm Z}(\mathbf{r}) = \gamma_{\rm Cu}\Delta B(\mathbf{r})$ (upper), and the EFG effect $\Delta\nu_{\rm EFG}(\mathbf{r}) = -A\Delta N(\mathbf{r})$ (lower). Parameters are the same as in Fig. 1.

At temperatures close to T_c, the space variation of the Zeeman effect is reduced following the reduced compression of the magnetic field in the vortex cores. Fig. 3 shows a decomposition of the lower NMR line into the Zeeman part and the EFG effect for $T = 0.9\ T_c$. One can see that here the amplitude of the EFG effect is close to the amplitude of the Zeeman effect. Note that the mean value of the EFG is larger than its spatial variation. This signals that the mean value provides a good approximation at this temperature.

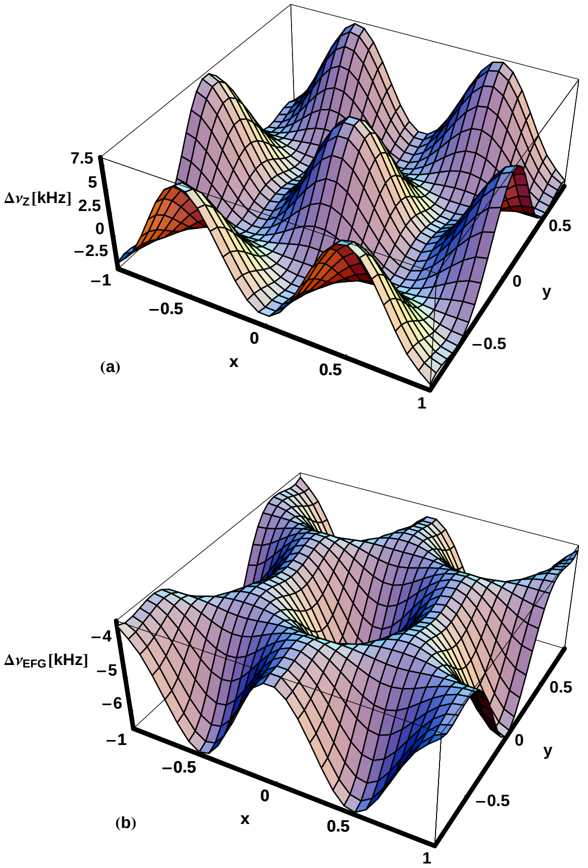

FIG. 3. The Zeeman effect $\Delta\nu_{\rm Z}(\mathbf{r}) = \gamma_{\rm Cu}\Delta B(\mathbf{r})$ (upper), and the EFG effect $\Delta\nu_{\rm EFG}(\mathbf{r}) = -A\Delta N(\mathbf{r})$ (lower), for $T = 0.9\ T_c$.

B. NMR lines of a single crystal

Above the critical temperature, the NMR lines of a single crystal are given by the Lorentzian distribution. Below T_c the space variation of the magnetic field deforms the lines so that their centers of mass (i.e., mean values) are not identical to their maxima, see Fig. 4.

The deformation of the NMR line seen in Fig. 4 can be correlated with the space distribution of the NMR frequency presented in Fig. 1. The vortex cores supply frequencies in the range from zero to 75 kHz above the mean value. Their contribution is visible as the extended left shoulder of the line in Fig. 4. The intermediate region between vortices supplies frequencies about 25 kHz below the mean value. Their contribution results in a shift of the maximum of the NMR line.

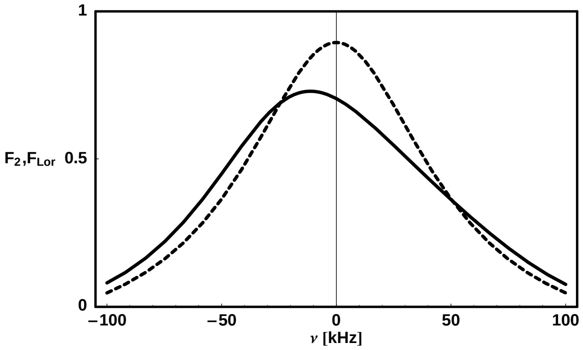

FIG. 4. The distribution $F_2(\nu)$ (solid line) compared with the Lorentz distribution $F_{\rm Lor}(\nu) = \frac{1}{\pi}\frac{\Gamma}{\nu^2+\Gamma^2}$ (dashed line) at $T = 0.6\ T_c$ and $\Gamma = 50$ kHz. The experimental line width is $\Gamma = 140$ kHz. We use the narrow line to make its deformation more visible.

The temperature dependence of the mean values $\langle\Delta\nu_{2,3}\rangle$ and the maxima $\Delta\bar{\nu}_{2,3}$ is presented in Fig. 5.

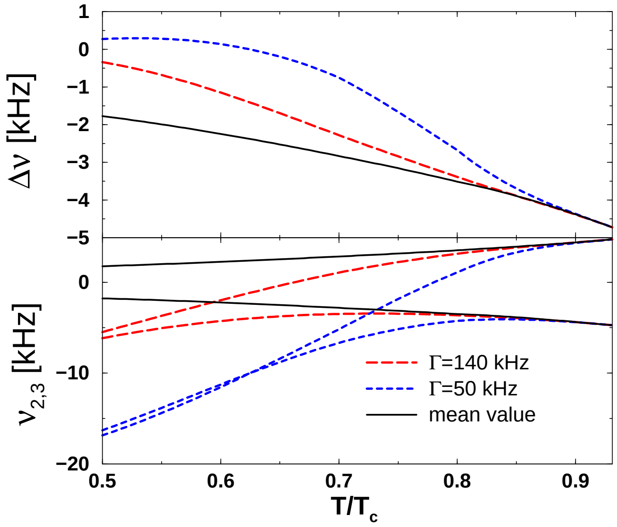

FIG. 5. The maxima $\bar{\nu}_{2,3}$ (dashed lines) and mean values $\langle\Delta\nu_{2,3}\rangle$ (full lines) of the lower and upper NMR lines (below) as a function of temperature. The corresponding shifts, $\Delta\bar{\nu} = \frac{1}{2}\left(\Delta\bar{\nu}_2 - \Delta\bar{\nu}_3\right)$ and $\langle\Delta\nu\rangle = \frac{1}{2}(\langle\Delta\nu_3\rangle - \langle\Delta\nu_2\rangle)$ are plotted above.

The mean value is independent of the space variation of the magnetic field, $\langle\Delta\nu_{2,3}\rangle = \gamma_{\rm Cu}\langle\Delta B\rangle \mp A\langle\Delta N\rangle = \mp A\langle\Delta N\rangle$, because $\langle\Delta B\rangle = 0$ by definition. The difference between the mean value and maximum thus shows the effect of the spatial variation of the magnetic field on the position of the maximum. Since the mean value is proportional to the charge transfer while the position of the maximum is a rather complicated quantity, the temperature region in the vicinity of T_c is more recommendable for the experimental exploration. We reserve the symbol T_c for the critical temperature in the absence of the magnetic field, $T_c = 90$ K. In the magnetic field $B = 9.4$ T, the actual phase transition is at $T = 0.931\ T_c$.

The deviation of the maximum from the mean value depends on the line width. This is illustrated in Fig. 5 by the line of artificially chosen width $\Gamma = 50$ kHz. In the limit of very broad lines, $\Gamma \to \infty$, the position of the maximum becomes identical to the mean value. This trend is also seen from the formula (4).

C. Conventional model

Let us make a small detour and assume that there is no charge transfer between chains and planes. In other words, no screening by chains is assumed and the charge is transfered exclusively inside the CuO_2 planes. In this case the system would behave as a conventional superconductor in which the charge is transfered from the vortex cores into the region between them. In this model, the charge density is given by $\rho_p = \varphi_p / L_{pp}$, while other relation remain the same as in the case of the above layered model.

One can see in Fig. 6 that the sign of $\Delta\nu$ is opposite to the sign of the model with screening by chains. Also, the magnitude of $\Delta\nu$ is extremely small. A typical shift is less than 1 Hz while the typical shift is more then 1 kHz in the case where the chains are accounted for. The values observed by KNM are about 10 kHz. Our result thus confirms the estimate of KNM that the conventional model of the vortex charge fails to explain their experimental data.[13]

When the transfer between chains and planes is prohibited, the amplitude is reduced by two mechanisms. First, the charge transfer accross the vortex core happens on a distance which is much larger than the distance between chains and planes. Second, the mean value of the shift is zero, $\langle \nu_i \rangle = 0$, because the charge of planes is conserved, $N_0 - \langle N \rangle = 0$. The line shift thus results merely from the statistical variations which are small due to the large line width, see (4).

An explanation of the reversed sign follows the argument given already by KNM.[13] Since the magnetic field is much smaller than H_{c2}, the area of vortex cores is much smaller than the area between them. Accordingly, cores have a negligible weight in statistical variations so that the charge between cores determines the line shift. This charge is opposite to the charge of cores, consequently the reversed sign of the line shift results from the conventional model.

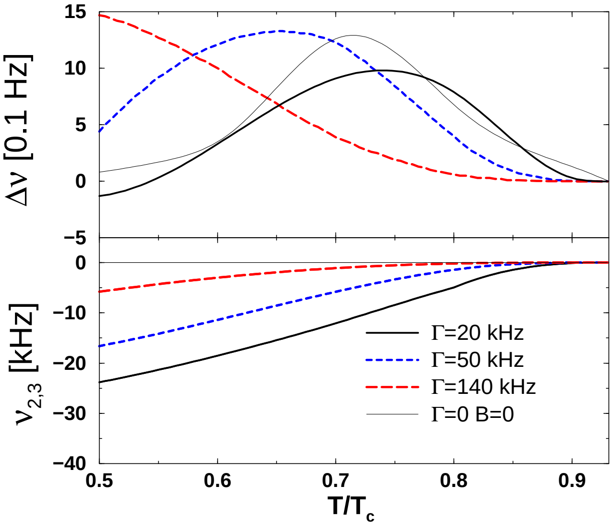

FIG. 6. The maxima $\bar{\nu}_{2,3}$ of the lower and upper NMR lines as a function of temperature (below) and the shift $\Delta\nu$ (above) in the absence of screening chains.

D. Averaging over grain orientation

As mentioned, KNM have used a granular sample with a high but not perfect orientation of YBCO grains.[13] The averaging over the grain orientation (39) results in an additional shift of the NMR frequencies, see Fig. 7. The grain disorientation contributes mainly at low temperatures where it leads to shifts of about 5 kHz, while the value predicted for the single crystal reduces with temperature.

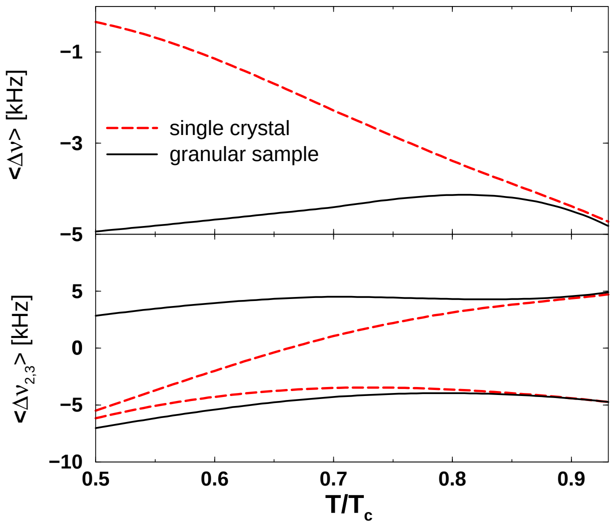

FIG. 7. The maxima $\Delta\bar{\nu}_{2,3}$ of the lower and upper NMR lines as a function of temperature (below) and the shift $\langle \Delta\nu \rangle$ (above) of $\Gamma = 140$ kHz of Fig. 5 compared with the averaging over grain boundaries according to (39).

Figure 8 compares our theoretical results with the experimental data of KNM. Apparently, the agreement is only qualitative. We have obtained the correct sign but the theoretical amplitude is about two or three times smaller than observed.

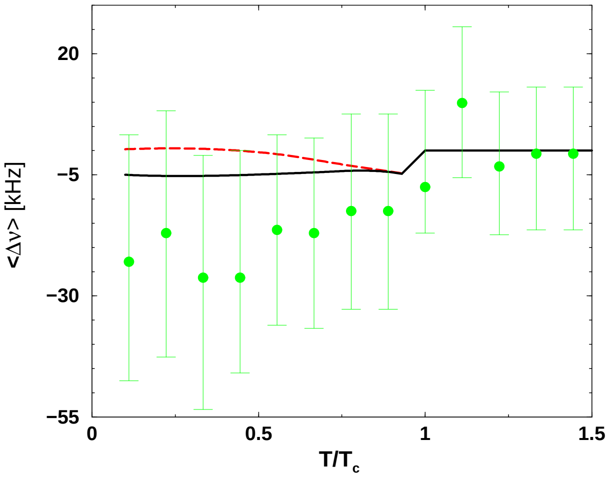

FIG. 8. Comparison of the theory with experiment. The experimental data are the dots with error bars, the theoretical prediction is the full line and the theoretical value for the single crystal is shown as a dashed line.

In the temperature dependence one can identify three regions. Above the critical temperature there is no charge transfer between chains and planes. Indeed, neglecting the second terms in the potential (23) we have neglected the thermally induced charge transfer in the normal state which appears for unequal energy derivatives of the density of states, $\partial\gamma_p/\partial n_p \neq \partial\gamma_c/\partial n_c$. The experimental data of KNM[13] above the critical temperature justify this neglect.

In the narrow region between T_c and 0.93 T_c the sample is superconducting only if the magnetic field is absent. The NQR frequency is thus measured in the superconducting state while the NMR frequencies are measured in the normal state. In this temperature region the observed frequencies are free of space fluctuations giving a direct experimental access to the charge transfer caused by the superconducting transition. Since in both cases (NMR and NQR) the magnetic field and the transfered charge are homogeneous, the averaging over the grain orientation is the same as in the normal state above T_c. Accordingly, the granular sample used by KNM should provide data comparing well with the single crystal. Unfortunately, this region is not covered by sufficiently detailed data in Ref. 13.

The region between 0.93 T_c and T_c can be used to experimentally test our assumption about the charge transfer between chains and planes. In the absence of the charge transfer between chains and planes, the shift $\Delta\nu$ is exactly zero since there are no vortices to cause the in-plane transfer.

Below 0.93 T_c the sample is superconducting even in the presence of the magnetic field, i.e., the Abrikosov vortex lattice enters the game. Let us first discuss the mean value. When the magnetic field penetrates the sample, the superconductivity is suppressed in the vortex cores. The charge transfer induced by vortices is crudely proportional to the product of the superconducting fraction and the area of the vortex core. As the temperature is reduced, the superconducting fraction grows while the diameter of the vortex cores shrinks down. For a GL parameter κ independent of the temperature, the product remains constant. Within Bardeen's approximation the GL parameter κ slightly decreases with the temperature,[12] therefore, the charge transfer reduces as $T \to 0$.

At temperatures below 0.7 T_c the maximum of the NMR line in the granular sample is strongly shifted by the angular averaging. According to our results, the granular samples in this temperature region cannot be used to access material properties.

VI. SUMMARY

We have shown that the experimental results of Kumagai, Nozaki and Matsuda can be explained in terms of a standard theory of the electrostatic field in superconductors extended by features necessary to describe the layered structure of YBCO. The agreement of our theory with the experiment is only qualitative. Our results thus do not exclude possible alternative mechanisms[23,24].

In conclusion, the charge transfer between CuO chains and CuO$_2$ planes in YBa$_2$Cu$_3$O$_7$ provides a qualitative explanation of the electric field gradient effect on the NMR lines. At low temperatures the effect of the charge transfer is spoiled by two additional effects: the space modulation of the Zeeman effect reduces the shift of the maxima of the NMR lines; the disorientation of grains in the sample increases the shift. From this point of view it is advisable to make precise measurement near the critical temperature where the charge transfer dominates.

Our study does not cover two realistic features that can increase the amplitude of the observed shift of NMR lines towards the experimental values. First, the charge is transfered from the copper to the apex oxygen, i.e., the distance between planes and chains $D_{cp} = 4.24$ Å should be reduced to the Cu-O distance 2.3 Å. This will enhance the charge transfer by a factor 1.8. We did not include this simple correction as its consistent implementation requires to use the non-local dielectric function and the microscopic treatment of electronic states. A similar type of enhancement would result from a higher value of the dielectric constant. We have used $\epsilon = 4\epsilon_0$ while values as large as $\epsilon = 100\epsilon_0$ has been advocated.[25] Second, the magnetic anisotropy of YBCO enhances the deviations of the magnetic field from the axes c in individual grains. At low temperatures this effect should be stronger in agreement with the observed trends. This correction is omitted because of an unknown vortex pinning.

It is apparent from the experimental data of KNM that an explanation of the NMR lines in the underdoped $YBa_2Cu_4O_8$ will be more complicated. Unfortunately, we could not discuss $YBa_2Cu_4O_8$, because we have not found a relevant set of material parameters.

ACKNOWLEDGMENTS

Authors are grateful to K. I. Kumagai, Y. Matsuda, P. Novák and J. Rosa for fruitful discussions. This work was supported by MŠMT program Kontakt ME601 and Grants Nos. GAČR 202000643, GAAV A1010806 and A1010919. The European ESF program VORTEX and the support by the Max-Planck society are gratefully acknowledged.

APPENDIX A: INNATE PERPENDICULAR MAGNETIC FIELD

The magnetic field perpendicular to the axis c appears in the sample from two sources. First, the observed samples are made from many grains with a small but finite scatter of the orientation of the c axis. This contribution is discussed in the main text. Second, since diamagnetic currents are in planes, the magnetic field is more compressed in layers of planes than in layers of chains. This part of the perpendicular field is innate to the layered system and appears also in single crystals.

Here we show that the innate perpendicular magnetic field can be neglected. The magnetic field is given by the vector potential $\mathbf{A}$. For $\mathbf{B} \parallel c$, the component of $\mathbf{A}$ along the c axis is zero, see (17). The perpendicular magnetic field thus reads,

$$B_x = -\frac{\partial A_y}{\partial z}, \qquad B_y = \frac{\partial A_x}{\partial z}. \tag{A1}$$

In the short notation, $\mathbf{B}_\perp = \hat{\mathbf{z}} \times \partial_z \mathbf{A}$, where $\hat{\mathbf{z}}$ is the unit vector in the direction z.

The vector potential (17) has a cusp at the positions of layers. This cusp appears due to the singular 2D current of the selected layer, say at z_j^+. From the mirror symmetry follows that the current in the z_j^+-layer does not contribute to the perpendicular magnetic field in the center of this layer, i.e., at z_j^+ where the Cu nuclei sit. We can thus avoid the cusp by taking neighbor layers only. The mirror symmetry also shows that all equivalent $z_{j'}^+$ layers spaced symmetrically above and below z_j^+ give zero net contribution. Accordingly, the perpendicular magnetic field in the vicinity of z_0^+ (for $|z - D_{pp}/2| \ll D_{pp}/2$) is given by the reduced vector potential,

$$\mathbf{A}^{\rm red}(\mathbf{r}, z) = \frac{\mu_0}{4\pi} \int d\mathbf{r}' \sum_{j'} \frac{\mathbf{j}_{j'}^-(\mathbf{r}')}{\sqrt{|\mathbf{r}' - \mathbf{r}|^2 + (z_{j'}^- - z)^2}}. \tag{A2}$$

The 2D Fourier transformation of (A2) yields

$$\mathbf{A}^{\rm red}(\mathbf{k}, z) = \frac{\mu_0}{2k} \frac{\mathrm{e}^{-k(z+D_{pp}/2)} + \mathrm{e}^{-k(D-z-D_{pp}/2)}}{1 - \mathrm{e}^{-kD}} \mathbf{j}_p(\mathbf{k}). \tag{A3}$$

The derivative of $\mathbf{A}^{\rm red}$ with respect to z at $z = D_{pp}/2$ provides us with the perpendicular magnetic field in terms of the 3D current, $\mathbf{j} = 2\mathbf{j}_p/D$,

$$\mathbf{B}_\perp = -\frac{\mu_0 D}{4} \frac{\mathrm{e}^{-kD_{pp}} - \mathrm{e}^{-k(D-D_{pp})}}{1 - \mathrm{e}^{-kD}} \hat{\mathbf{z}} \times \mathbf{j}(\mathbf{k}). \tag{A4}$$

Let us estimate the value of the perpendicular field. To this end we employ the long wave length limit, $k \to 0$,

$$\mathbf{B}_\perp \approx -\frac{\mu_0}{4}(D - 2D_{pp}) \hat{\mathbf{z}} \times \mathbf{j}(\mathbf{k}). \tag{A5}$$

The maximum of the current is at the edge of the vortex core, i.e., at $r \approx \sqrt{2}\xi$, where $\xi = \lambda/\kappa$ is the GL coherence length. The amplitude of the vector potential at this point, $A = \Phi_0/(2\pi r) = \Phi_0\kappa/(2\pi\sqrt{2}\lambda)$, gives the current density $\mu_0 j = A/\lambda^2 = \Phi_0\kappa/(2\sqrt{2}\pi\lambda^3)$. For the YBCO parameters, $(D - 2D_{pp})/4 = 1.33$ Å, $\kappa = 55$, and $\lambda = 1400$ Å, one finds $B_\perp \approx 6 \times 10^{-4}$ T. This field is far too small shifting the NMR line by $\nu_0 \frac{3}{2} \sin^2\theta \approx 0.2$ Hz. We have used $\nu_0 = 31.5$ MHz.

---

[1] G. Rickayzen, J. Phys. C **2**, 1334 (1969).

[2] J. Bok and J. Klein, Phys. Rev. Lett. **20**, 660 (1968).

[3] J. B. Brown and T. D. Morris, Proc. 11th Int. Conf. Low. Temp. Phys., Vol. 2, 768 (St. Andrews, 1968).

[4] T. D. Morris and J. B. Brown, Physica **55**, 760 (1971).

[5] Yu. N. Chiang and O. G. Shevchenko, Fiz. Nizk. Temp. **12**, 816 (1986) [Low. Temp. Phys. **12**, 462 (1986)].

[6] Yu. N. Chiang and O. G. Shevchenko, Fiz. Nizk. Temp. **22**, 669 (1996) Low. Temp. Phys. **22**, 513 (1996)].

[7] P. Lipavský, J. Koláček, J. J. Mareš and K. Morawetz, Phys. Rev. B **65**, 012507 (2001).

[8] D. I. Khomskii and F. V. Kusmartsev, Phys. Rev. B **46**, 14245 (1992).

[9] D. I. Khomskii and A. Freimuth, Phys. Rev. Lett. **75**, 1384 (1995).

[10] G. Blatter, M. Feigel'man, V. Geshkenbein, A. Larkin and A. van Otterlo, Phys. Rev. Lett. **77**, 566 (1996).

[11] J. Koláček and P. Lipavský, Physica C **364**, 138 (2001).

[12] P. Lipavský, J. Koláček, K. Morawetz and E. H. Brandt, Phys. Rev. B **65**, 144511 (2002).

[13] K. I. Kumagai, K. Nozaki and Y. Matsuda, Phys. Rev. B **63**, 144502 (2001).

[14] H. Yasuoka, in *Spectroscopy of Mott Insulator and Correlated Metals*, editted by A. Fujimori and Y. Tokura, Solis State Sciences **119**, 213 (Springer-Verlag, Berlin 1995).

[15] W. E. Lawrence and S. Doniach, in *Proc. of the 12th Int. Conf. on Low-Temperature Physics*, Kyoto, 1970, edited by E. Kanda (Keigaku, Tokyo, 1971), p. 361.

[16] I. N. Bulaevskii, Int. J. of Modern Physics B **4**, 1849 (1990).
[17] J. Bardeen, Phys. Rev. **94**, 554 (1954).
[18] J. Bardeen, *Theory of Surperconductivity* in Handbuch der Physik, Bd. XV. (1955).
[19] E. H. Brandt, Phys. Rev. Lett. **78**, 2208 (1997).
[20] C. P. Slichter, *Principles of Magnetic Resonance* (Springer-Verlag, Berlin 1978).
[21] N. M. Plakida, *High-Temperature Superconductivity* (Springer-Verlag, Berlin 1995).
[22] A. Junod, in *Physical Properties of High Temperature Superconductors II*, ed. D. M. Ginsberg (World Scientific, Singapore 1990).
[23] E. Šimánek, Phys. Rev. B **65**, 184524 (2002).
[24] Y. Chen, Z. D. Wang, J.-X. Wang and C. S. Ting, The 2002 Int. Conf. on Phys. and Chem. of Molecular and Oxide Superconductors (MOS2002), August 13-18, 2002 in Hsinchu, Taiwan. To appear in J. Low. Temp. Phys.
[25] J. Mannhart, Mod. Phys. Lett. B **6**, 555 (1992).